Amplified spontaneous emission in graded-index polymer optical fibers: theory and experiment

M. Asunción Illarramendi,[1,*] Jon Arrue,[2] Igor Ayesta,[2] Felipe Jiménez,[3] Joseba Zubia,[2] Iñaki Bikandi,[2] Akihiro Tagaya,[4] and Yasuhiro Koike[4]

[1]*Department of Applied Physics I, University of the Basque Country (UPV/EHU), Escuela Técnica Superior de Ingeniería (ETSI) de Bilbao, Alda. Urquijo s/n, E-48013 Bilbao, Spain*
[2]*Department of Communications, UPV/EHU, ETSI de Bilbao, Alda. Urquijo s/n, E-48013 Bilbao, Spain*
[3]*Department of Applied Mathematics, UPV/EHU, ETSI de Bilbao, Alda. Urquijo s/n, E-48013 Bilbao, Spain*
[4] *Faculty of Science and Technology, Keio University, 3-14-1 Hiyoshi, Kohoku-ku, Yokohama 223-0061, Japan*
[*]*ma.illarramendi@ehu.es*

Abstract: In this work we analyze experimentally and theoretically the properties of amplified spontaneous emission (ASE) in a rhodamine-6G-doped graded-index polymer optical fiber. A theoretical model based on the laser rate equations describes the ASE features successfully. The dependence of the ASE threshold and efficiency on fiber length is analyzed in detail.

OCIS codes: (060.2310) Fiber optics; (060.3510) Lasers, fiber; (060.2320) Fiber optics amplifiers and oscillators; (160.2540) Fluorescent and luminescent materials; (250.3680) Light-emitting polymers.

References and links

1. J. Zubia and J. Arrue, "Plastic optical fibers: An introduction to their technological processes and applications," Opt. Fiber Technol. **7**(2), 101–140 (2001).
2. Y. Koike and M. Asai, "The future of plastic optical fiber," NPG Asia Mater. **1**(1), 22–28 (2009).
3. O. Ziemann, J. Krauser, P. E. Zamzow, and W. Daum, *POF Handbook: optical short range transmission systems*, 2nd ed. (Springer, 2008).
4. T. Kaino, "Polymer optical fibers," in *Polymers for Lightwave and Integrated Optics* (Marcel Deckker, Inc., 1992), Chap.1.
5. M. G. Kuzyk, *Polymer Fiber Optics: Materials, Physics, and Applications* (CRC Press, 2007).
6. J. Clark and G. Lanzani, "Organic photonics for communications," Nat. Photonics **4**(7), 438–446 (2010).
7. S. Muto, A. Ando, O. Yoda, T. Hanawa, and H. Ito, "Tunable laser using sheet of dye-doped plastic fibers," Electron. Commun. Jpn. **71**(Part II), 47–52 (1988).
8. A. Tagaya, Y. Koike, E. Nihei, S. Teramoto, K. Fujii, T. Yamamoto, and K. Sasaki, "Basic Performance of an Organic Dye-Doped Polymer Optical Fiber Amplifier," Appl. Opt. **34**(6), 988–992 (1995).
9. A. Tagaya, S. Teramoto, T. Yamamoto, K. Fujii, E. Nihei, Y. Koike, and K. Ssasaki, "Theoretical and Experimental Investigation of Rhodamine B-Doped Polymer Optical-Fiber Amplifiers," IEEE J. Quantum Electron. **31**(12), 2215–2220 (1995).
10. G. D. Peng, P. L. Chu, Z. Xiong, T. W. Whitbread, and R. P. Chaplin, "Dye-doped step-index polymer optical fiber for broadband optical amplification," J. Lightwave Technol. **14**(10), 2215–2223 (1996).
11. A. Tagaya, T. Kobayashi, S. Nakatsuka, E. Nihei, K. Sasaki, and Y. Koike, "High gain and high power organic dye-doped polymer optical fiber amplifiers: Absorption and emission cross sections and gain characteristics," Jpn. J. Appl. Phys. **36**(Part 1, No. 5A), 2705–2708 (1997).
12. K. Kuriki, T. Kobayashi, N. Imai, T. Tamura, S. Nishihara, Y. Nishizawa, A. Tagaya, Y. Koike, and Y. Okamoto, "High-efficiency organic dye-doped polymer optical fiber lasers," Appl. Phys. Lett. **77**(3), 331–333 (2000).
13. T. Kobayashi and W. J. Blau, "Laser emission from conjugated polymer in fibre waveguide structure," Electron. Lett. **38**(2), 67–68 (2002).
14. T. Kobayashi, W. Blau, H. Tillmann, and H. Horhold, "Light amplification and lasing in a stilbenoid compound-doped glass-clad polymer optical fiber," IEEE J. Quantum Electron. **39**(5), 664–672 (2003).
15. M. Karimi, N. Granpayeh, and M. Moravvej-Farshi, "Analysis and design of a dye-doped polymer optical fiber amplifier," Appl. Phys. B **78**(3-4), 387–396 (2004).
16. M. Sheeba, K. J. Thomas, M. Rajesh, V. P. N. Nampoori, C. P. G. Vallabhan, and P. Radhakrishnan, "Multimode laser emission from dye doped polymer optical fiber," Appl. Opt. **46**(33), 8089–8094 (2007).
17. M. Rajesh, M. Sheeba, K. Geetha, C. P. G. Vallaban, P. Radhakrishnan, and V. P. N. Nampoori, "Fabrication and characterization of dye-doped polymer optical fiber as a light amplifier," Appl. Opt. **46**(1), 106–112 (2007).
18. H. Liang, Z. Zheng, Z. Li, J. Xu, B. Chen, H. Zhao, Q. Zhang, and H. Ming, "Fabrication and amplification of rhodamine B-doped step-index polymer optical fiber," J. Appl. Polym. Sci. **93**(2), 681–685 (2004).

#193466 - $15.00 USD Received 5 Jul 2013; revised 6 Sep 2013; accepted 9 Sep 2013; published 3 Oct 2013

19. G. V. Maier, T. N. Kopylova, V. A. Svetlichnyi, V. M. Podgaetskii, S. M. Dolotov, O. V. Ponomareva, A. E. Monich, and E. A. Monich, "Active polymer fibres doped with organic dyes: Generation and amplification of coherent radiation," Quantum Electron. **37**(1), 53–59 (2007).
20. J. Clark, L. Bazzana, D. D. C. Bradley, J. Cabanillas-Gonzalez, G. Lanzani, D. G. Lidzey, J. Morgado, A. Nocivelli, W. C. Tsoi, T. Virgili, and R. Xia, "Blue polymer optical fiber amplifiers based on conjugated fluorene oligomers," J. Nanophotonics **2**(1), 023504 (2008).
21. M. J. F. Digonnet, *Rare-Earth-Doped Fiber Lasers and Amplifiers, Revised and Expanded*, 2nd ed., (Marcel Dekker, Inc., 2001).
22. J. Arrue, F. Jiménez, M. A. Illarramendi, J. Zubia, I. Ayesta, I. Bikandi, and A. Berganza, "Computational Analysis of the Power Spectral Shifts and Widths Along Dye-Doped Polymer Optical Fibers," IEEE Photonics J. **2**(3), 521–531 (2010).
23. J. Arrue, F. Jimenez, I. Ayesta, M. A. Illarramendi, and J. Zubia, "Polymer-Optical-Fiber Lasers and Amplifiers Doped with Organic Dyes," Polymers **3**(4), 1162–1180 (2011).

1. Introduction

Polymer optical fibers (POFs) are well known in the field of fiber optics thanks to their robustness, large core diameters, high numerical apertures and low cost [1]. In the last few years POFs have been widely used both for short-haul communications links, in which distances are generally shorter than one kilometer, and for a wide variety of sensing applications [2–4]. On the other hand, the possibility of doping POFs with functional materials has opened a wide range of new applications for optical fibers in the fields of lasers, amplifiers, switches and sensors in the visible region [5,6]. As is well-known, the lower manufacturing temperatures of POFs as compared to glass fibers make it possible to embed a wide range of available materials into the fiber core. Fiber-waveguide structures provide optical confinement in the core area and a long interaction distance between the light and the gain medium. In addition, they yield a symmetric output of the beam profile, a good adaptability to fiber-optic communications systems and a high ratio between surface area and volume, which allows efficient heat dissipation and minimization of thermal degradation of performance. All these properties make optical fibers suitable for achieving efficient lasing and amplification devices.

Since the discovery in 1987 of a fiber-type laser based on a dye-doped polymer fiber [7], active POFs doped with organic dyes or with organic semiconductors have been studied extensively [8–20]. The interest of organic dyes in POFs lies in their extraordinary large emission and absorption cross sections, which allow interaction with light in much shorter distances than those achieved with traditional rare-earth dopants. Most of these works analyze the use of POFs as optical fiber amplifiers, which yield high gains for a launched signal [8–11,15,17,18,20]. On the contrary, there have been few reports about amplified spontaneous emission (ASE) and lasing performance in doped POFs. In addition, none of these reports analyzes the experimental results obtained theoretically. Although both conventional fiber lasers and mirrorless ones rely on the amplification of stimulated emission, the former ones employ an optical resonator that filters the ASE yielding a narrow emission spectrum, whereas the latter ones do not utilize such a resonator and they simply emit ASE. Since the ASE power is generally broadband, doped fibers based on ASE can be used as broadband fiber sources, such as those sources preferable in fiber gyroscopes [21].

In this work, we present a detailed experimental and theoretical study of the properties of the ASE phenomenon in a graded-index (GI) POF doped with rhodamine 6G (R6G). The pump threshold for the onset of ASE and the efficiency have been measured and analyzed as functions of the fiber length. The theoretical model has been carried out by means of the rate equations for the light power and the electronic population, in terms of time, distance traveled by light and wavelength. In the analysis, it has been taken into account that the fiber analyzed is a typical GI POF in which the radial distributions of light power density and dye density are not uniform. The main goal of this work is to show together, for the first time, experimental and theoretical results of the ASE phenomenon in a doped GI POF, allowing us to explain the results obtained. For this purpose, simple analytical expressions have also been derived.

#193466 - $15.00 USD Received 5 Jul 2013; revised 6 Sep 2013; accepted 9 Sep 2013; published 3 Oct 2013

2. Experimental

The samples analyzed are GI POFs doped with rhodamine 6G, which were prepared in the way described in [11]. The diameter of the fiber core is 0.6 mm and the total fiber diameter including the cladding is 1 mm. As the fiber is GI, the light power density ψ (power per unit area) is greater in the proximity of the fiber symmetry axis. Its variation with the radial distance r can be seen in Fig. 1 [9]. The dopant concentration is also greater in the proximity of $r = 0$, and its radial normalized variation ($N(r)/N(0)$) is also shown in Fig. 1.Its average value in the fiber core is, approximately, 12 ppm in weight, and the cladding material is not doped. The refractive index at the fiber symmetry axis is $n_1 = 1.501$, and it decreases to 1.492 in the cladding with a typical clad-power-law profile. Depending on the measurement, the fiber samples were cut into appropriate lengths L (2-30 cm), and, in all cases, the fiber ends were carefully polished by hand with polishing papers.

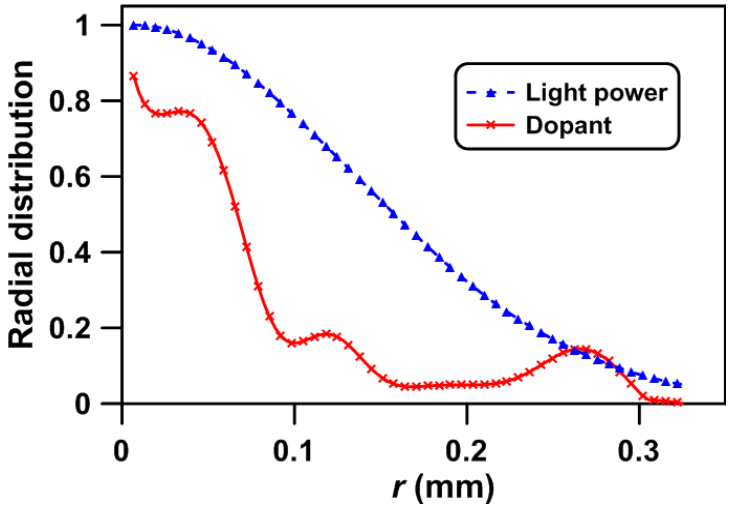

Fig. 1. Normalized radial distributions of light power density ($\psi(r)/\psi(0)$) and of dopant density ($N(r)/N(0)$) in the fiber core.

The emission spectra of the doped fiber were measured at room temperature by using as light source the frequency doubled output (532 nm) of a 10 Hz Q-switched Nd:YAG laser (EKSPLA NL301HT). The duration of the pump pulse was about 20 ns, and the pulse energy was controlled by insertion of calibrated neutral density filters into the beam path. The pump energy was measured with a calibrated pyroelectric energy detector (Newport 818E-10-50-S). Figure 2 illustrates the optical set-up used to measure the optical spectra from the end of the samples upon longitudinal excitation. The laser beam was focused onto the fiber end at normal incidence with a spot size of 1 mm by using a convergent lens of 50 cm of focal length. The measured doped fiber was held between two *xy*-micropositioners to maintain the fiber totally horizontal and to focus the incident laser beam on the fiber correctly. The output spectra from the fiber end opposite the pump input were recorded with a fiber-optic spectrometer (Ocean Optics USB4000) with an optical resolution of 1.5 nm of full width at half maximum. When the output light intensity was too large, neutral density filters were inserted in a filter holder in front of the spectrometer. The holder (Avantes FH-Inline-1") had two quartz collimating lenses and two SMA 905 connectors to facilitate light coupling into the spectrometer. In addition, in order to remove the pump power that could propagate through the fiber, a 532 nm long-pass edge filter was inserted in the filter holder. All the emission spectra were corrected for the response of the detection system, including the filters. The absorption spectrum of the doped fiber was recorded on a Cary 50 UV-Vis spectrophotometer equipped with a fiber-optic-coupler accessory. In this measurement the

#193466 - $15.00 USD Received 5 Jul 2013; revised 6 Sep 2013; accepted 9 Sep 2013; published 3 Oct 2013

length of the fiber was 1.3 cm, so that the absorption band of the R6G molecules embedded in the fiber could be detected.

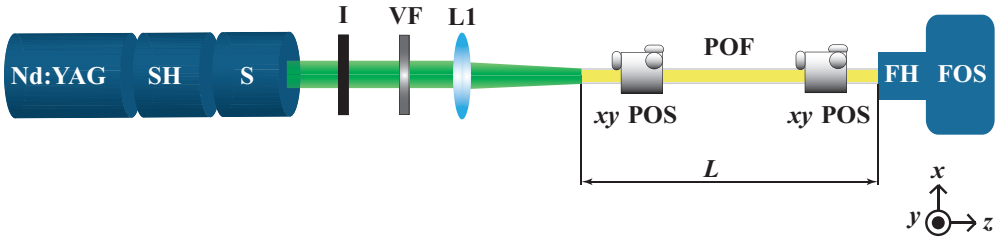

Fig. 2. Experimental set-up used to measure the emitted intensity in the doped GI POF. Legend: Nd:YAG: laser; SH: second harmonic generator; S: harmonic beam separator; I: iris; VF: variable absorptive neutral densitive filter; L1: bi-convex lens ($f' = +50$ cm); *xy* POS: *xy*-micropositioner; FH: filter holder; FOS: fiber-optic spectrometer.

3. Theoretical model

Light generation and amplification in GI POFs doped with R6G can be described by the rate equations for two energy levels. For the longitudinal excitation employed, the partial differential equations that determine light power along the different points z of the fiber, at any instant t, and also as a function of the light wavelength, are the following ones [22,23]:

$$\frac{\partial P_p}{\partial z} = -\sigma^a(\lambda_p) N_1 P_p \gamma - \frac{1}{v_z}\frac{\partial P_p}{\partial t} \tag{1}$$

$$\frac{\partial N_2}{\partial t} = \frac{-N_2}{\tau} - \left(\frac{\sigma^e(\lambda_k)}{h(c/\lambda_k)A_{core}}\right) N_2 P \gamma + \left(\frac{\sigma^a(\lambda_p)}{h(c/\lambda_p)A_{core}}\right) N_1 P_p \gamma + \left(\frac{\sigma^a(\lambda_k)}{h(c/\lambda_k)A_{core}}\right) N_1 P \gamma \tag{2}$$

$$\frac{\partial P}{\partial z} = \sigma^e(\lambda_k) N_2 P \gamma - \sigma^a(\lambda_k) N_1 P \gamma - \frac{1}{v_z}\frac{\partial P}{\partial t} + \frac{N_2}{\tau}\left(h\frac{c}{\lambda_k}\right)\sigma^e_{sp}(\lambda_k)\beta A_{core} \tag{3}$$

where $P_p(t,z)$ is the power at the pump wavelength λ_p and $P(t,z,\lambda_k)$ is the emission power at each of the wavelengths λ_k. N_2 is the density of the dye molecules in the excited state. The total density of dye molecules is $N = N_1 + N_2$, where N_1 accounts for the population in the ground energy level; v_z is the average speed of light in the medium, which depends on the refractive-index profile for each wavelength, c is the speed of light in the vacuum, h is Planck's constant, τ is the excited state lifetime, and A_{core} is the section of the fiber core. γ is an overlapping factor that must be introduced into the equations to take into account that light interacts more efficiently with the dopant in GI POFs because the light power density and the dopant concentration are both greater in short radial distances (see Fig. 1). If the dopant concentration were uniform in the core, γ would be equal to 1. However, when the dopant distribution is more concentrated towards the fiber symmetry axis, its interaction with light increases, yielding values of γ greater than 1 [23]. The exact value of γ ranges between 1 and 2 for a typical radial light distribution in a GI POF, but it could be greater in a fiber prepared ad hoc in which the light power distribution were narrower, with the majority of the dopant concentrated very near the fiber symmetry axis. β is the fraction of spontaneous emissions contributing to the amplification process. It is calculated as the fraction of spontaneously emitted power that lies in guided directions in the positive propagation sense ($z+$). The propagation of light in the negative sense ($z-$) has not been considered, since the amount of power eventually generated towards the positive sense ($z+$) as a consequence of such light is much smaller than the directly generated power [21]. Since the fibers considered in this paper are GI ones, the value of β has been calculated as a weighted average for all radial distances in the cross section [23], including the contribution of spontaneous emissions that are not lost

#193466 - $15.00 USD Received 5 Jul 2013; revised 6 Sep 2013; accepted 9 Sep 2013; published 3 Oct 2013

due to reflections in the cladding-air interface. The spectral dependence due to the dopant is introduced by means of the wavelength-dependent absorption and emission cross sections, namely $\sigma^{a}(\lambda_k)$, $\sigma^{e}(\lambda_k)$ and the probability of spontaneous emissions $\sigma_{sp}^{e}(\lambda_k)$.The numerical resolution of Eqs. (1-3) is carried out for each of the emission wavelengths considered λ_k, which are the centers of the discrete subintervals into which the spectrum is divided.

As for the boundary conditions, the pump pulse is Gaussian with a certain full width at half maximum (FWHM). Its equation is given by:

$$P_p(z{=}0,t) = \frac{E_p}{\sigma\sqrt{2\pi}} e^{-\frac{(t-t_{peak})^2}{2\sigma^2}} \tag{4}$$

where σ is the effective width (FWHM / 2.35), E_p is the energy of the pulse impinging on the fiber, and t_{peak} is taken to be equal to 4σ in order to have a negligible power at $t = 0$. The pump is launched at $z = 0$, which represents the point in the length L of fiber farthest from the photodetector. Finally, the emission power P is assumed to be 0 for all values of z at $t = 0$.

4. Results and discussion

In Fig. 3, we show the absorption spectrum of the fiber studied in the 300-1100 nm region. Apart from the strong absorption band corresponding to the dopant in the visible region, we can also observe the characteristic absorption bands of the PMMA matrix in the near infrared region. The maximum absorption for R6G in the fiber occurs at wavelengths between 490 and 556 nm. The fluorescence spectrum of a fiber with L = 2.5 cm is also plotted in the same figure. It should be noticed that there is a strong overlap between the absorption and fluorescence spectra. This fact will cause shifts in the emission wavelengths when the fiber length is changed.

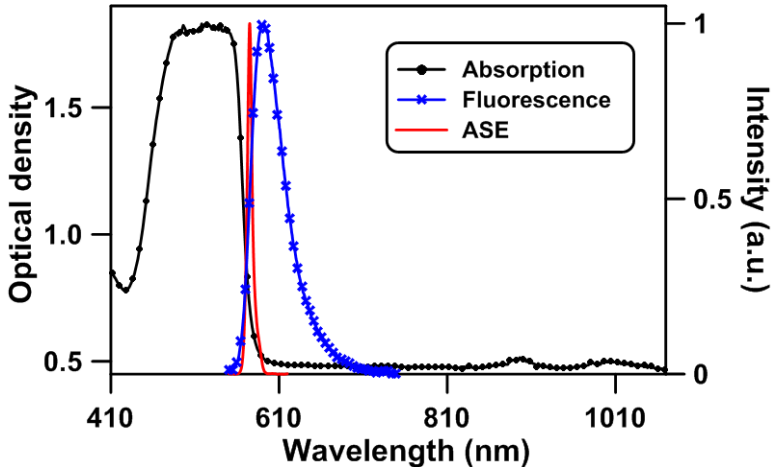

Fig. 3. Absorption spectrum and two normalized emission spectra at different pump energies for our R6G-doped GI POF. The emission spectra have been obtained by exciting the fiber longitudinally with L = 2.5 cm at pump energies below the threshold (fluorescence, E_p = 1.5 μJ) and above the threshold (ASE, E_p = 3.7 mJ).

Figure 4 illustrates the ASE performance in POFs of different fiber lengths excited longitudinally with pump energies ranging from 0 to nearly 4 mJ. It should be noticed that the output energies in Fig. 4 correspond to the total spectrum of the emission, i.e. they are integrated for all emitted wavelengths. From these measurements, we have determined the ASE threshold and the efficiency for each length. The threshold value is calculated from the intersection between the x axis and the straight line that best fits the values once they are growing rapidly; and the efficiency is the slope of that line. Figures 5(a) and 5(b) show, respectively, the abrupt blue shift in the average wavelength λ_{av} of the emission spectrum and

#193466 - $15.00 USD Received 5 Jul 2013; revised 6 Sep 2013; accepted 9 Sep 2013; published 3 Oct 2013

the narrowing in its width as the pump energy is increased around the ASE threshold. The spectral narrowing can also be observed in Fig. 3, in which we have included the ASE spectrum for a value of E_p above the threshold (E_p = 3.7 mJ). For the fiber lengths analyzed, it can be seen that the threshold becomes higher (see Figs. 4 and 5) and that the efficiency drops (see Fig. 4) as the fiber length increases. In addition, in most of the curves of Fig. 5(a), it can be noted that the emission spectrum is shifted towards longer wavelengths as the fiber length is increased with the same pump energy, due to absorption and reemission processes that take place along the fiber. Above threshold, the opposite phenomenon, i.e. a shift towards shorter wavelengths, can occur [22].

The theoretically and experimentally obtained dependence of the ASE threshold and efficiency on the fiber length L is plotted in Figs. 6(a) and 6(b). Whereas the experimental thresholds are absolute values, the experimental efficiencies are relative ones, since these values have been normalized in Fig. 6(b) according to the theoretically calculated absolute ones. The theoretical calculations have been carried out by solving Eqs. (1-3) numerically using the method described in [22,23], with the following parameters: $\beta = 0.07$, $A_{core} = \pi\ 0.3^2$ mm^2, τ = 4.8 ns and FWHM = 20 ns. The shapes of the curves $\sigma^{a}(\lambda_k)$ and $\sigma^{e}(\lambda_k)$ have been calculated from the absorption and emission spectra measured in our own fiber (see Fig. 3). The absolute values of those curves have been determined using the peak values of the cross sections measured in PMMA bulk as detailed in [9]. These peak values are 4.3×10^{-20} m^2 for $\sigma^{a}(\lambda_k = 532\ \text{nm})$ and 1.7×10^{-20} m^2 for $\sigma^{e}(\lambda_k = 580\ \text{nm})$. The output energies, calculated at $z = L$, have been obtained by time integration of the powers at each generated wavelength and by adding the energies for all the emission wavelengths. The range of pump energies considered to calculate the efficiencies and thresholds in the theoretical calculations is the same as in the experimental measurements, i.e. from 0 to 4 mJ. Three different values of the overlapping factor γ have been considered: $\gamma = 1$, which is the limiting case corresponding to a uniform dopant distribution; $\gamma = 1.7$, which is the value of our fiber obtained from Fig. 1 as explained in [23]; and $\gamma = 3$, for the sake of comparison.

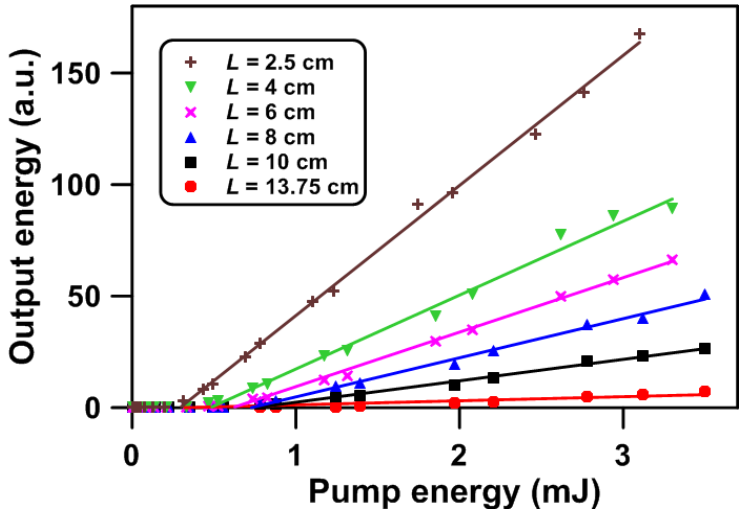

Fig. 4. Output emission energy integrated over all wavelengths as a function of pump energy in our doped GI POFs of various fiber lengths. The solid lines are the linear fits of the experimental points.

#193466 - $15.00 USD Received 5 Jul 2013; revised 6 Sep 2013; accepted 9 Sep 2013; published 3 Oct 2013

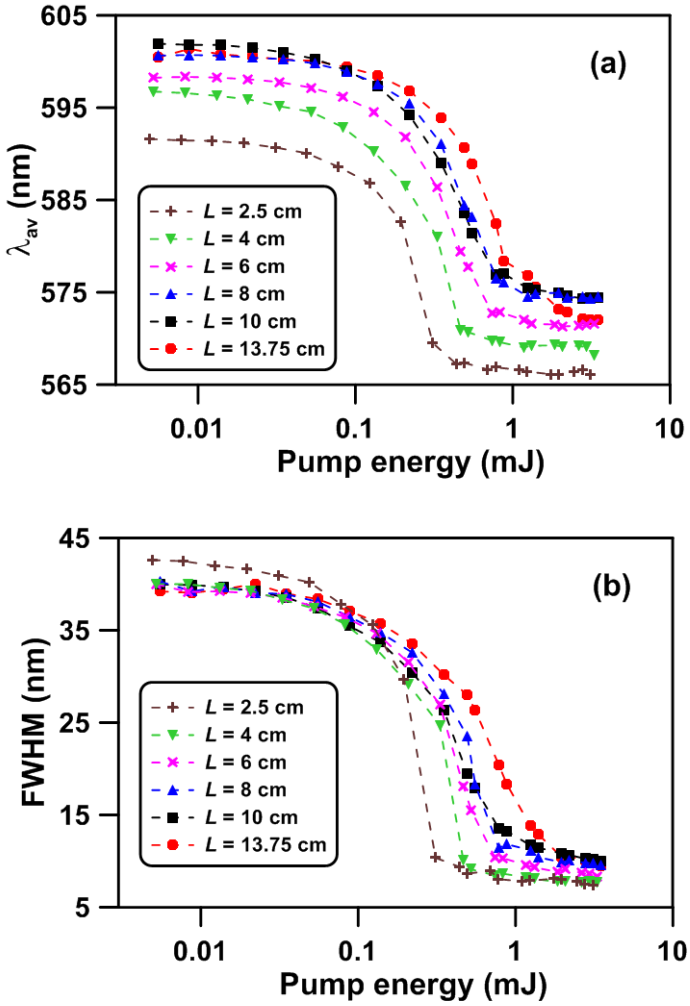

Fig. 5. (a) Shift of the average wavelength of the emission spectra, and (b) narrowing of their widths, as functions of pump energy in our doped GI POFs of various fiber lengths. The dashed lines serve to guide the eye.

In Fig. 6(a) we can see that the theoretical and experimental threshold energies tend to increase rather linearly with fiber length. Figure 6(b) shows the dependence of the efficiencies on fiber length. In all cases, the efficiencies tend to decrease exponentially when L is large enough. However, the efficiency could not be measured for the very short fibers that would show the initial increase in the curves obtained theoretically. At such short lengths, which are not reached due to constraints of our experimental setup, the theoretical efficiency increases rapidly with length up to a maximum. This optimum fiber length for maximum efficiency depends on γ and it is shorter if γ increases. For distances of about 2 cm or shorter, ASE thresholds cannot be calculated because the ASE efficiency is nearly 0. As can be seen in Fig. 6(a), the thresholds theoretically calculated for the three values of γ are of the same order of magnitude as the experimental ones, although they are slightly lower. This behavior could be due to extra losses (imperfections, reflections at the input interfaces, etc.) that are not considered in the model.

#193466 - $15.00 USD Received 5 Jul 2013; revised 6 Sep 2013; accepted 9 Sep 2013; published 3 Oct 2013

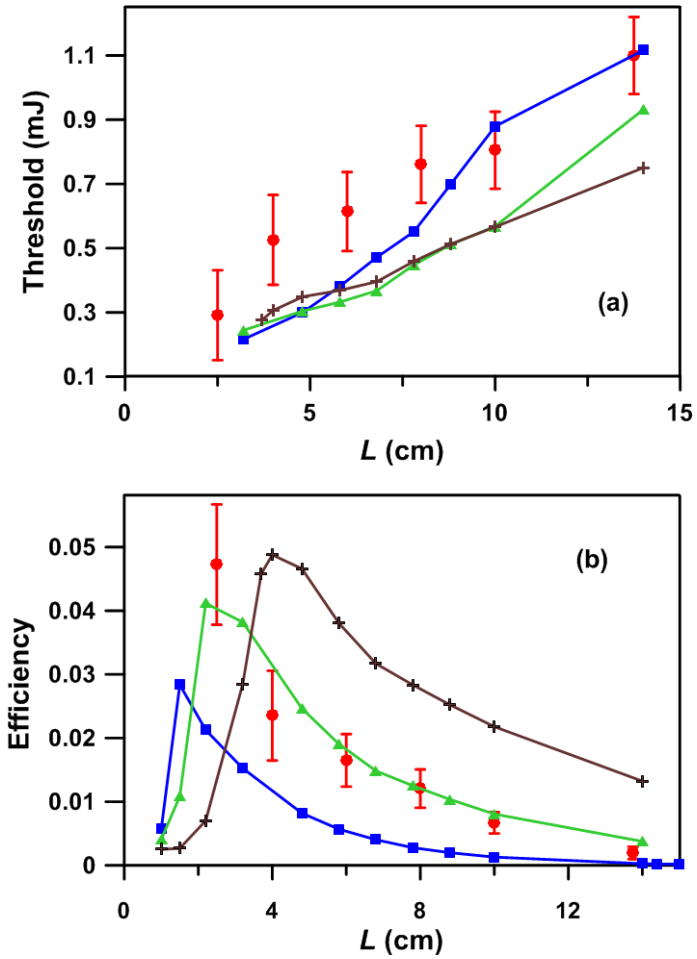

Fig. 6. Threshold (a) and efficiency (b) as functions of fiber length. Circles: experimental points. Solid lines with crosses: theoretical curves with $\gamma = 1$. Solid lines with triangles: theoretical curves with $\gamma = 1.7$. Solid lines with squares: theoretical curves with $\gamma = 3$. The theoretical efficiencies decay exponentially with coefficients: $\alpha = 0.12$ cm^{-1} ($\gamma = 1$), $\alpha = 0.21$ cm^{-1} ($\gamma = 1.7$), $\alpha = 0.38$ cm^{-1} ($\gamma = 3$). The experimental values of the efficiency in (b) have been normalized to the theoretical curve with $\gamma = 1.7$, which is the value that corresponds to our measured fiber.

The fact that the experimental threshold and efficiency worsen as the fiber length is increased can be explained by taking into account that the fiber lengths employed are greater than the length corresponding to the gain volume in the active fiber. This behavior is illustrated in Fig. 7, which shows the spatial distribution of the excited state population $N_2(z)$ from the point in the length L of the fiber farthest from the photodetector ($z = 0$) towards the photodetector ($z > 0$). This distribution would represent the gain region, and it has been calculated by time integration of the function $N_2(t,z)$.

#193466 - $15.00 USD Received 5 Jul 2013; revised 6 Sep 2013; accepted 9 Sep 2013; published 3 Oct 2013

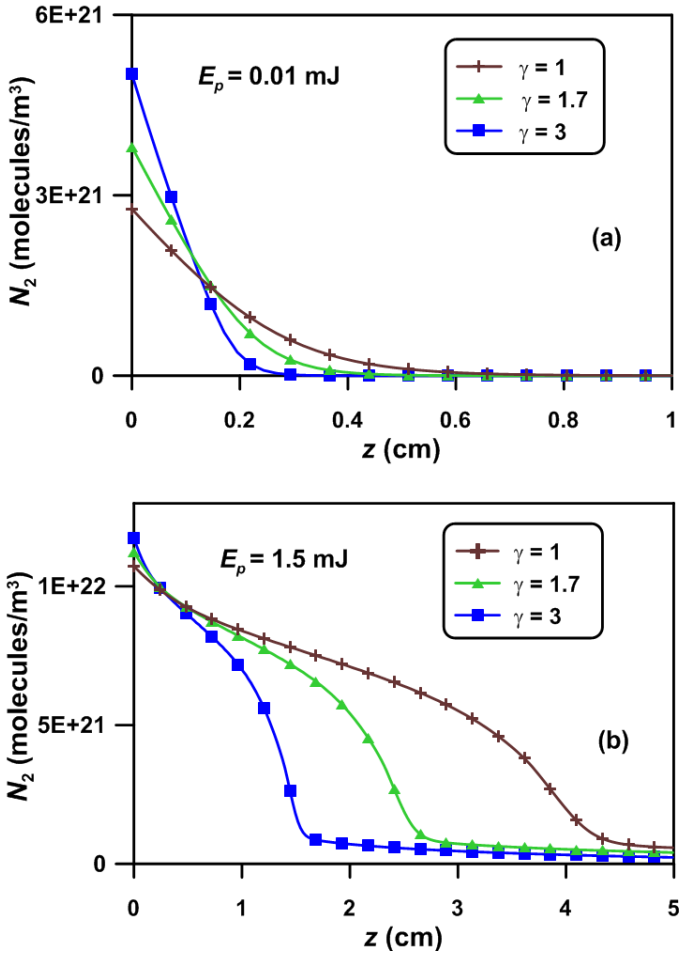

Fig. 7. Spatial distribution of N_2 for the overlapping factors considered. (a) Pump energy below threshold, E_p = 0.01 mJ. (b) Pump energy above threshold, E_p = 1.5 mJ.

In Fig. 7, the distributions corresponding to two pump energies have been compared for the three values of γ considered: a pump energy that is below the threshold, such as 0.01 mJ in Fig. 7(a), and another one above the threshold, such as 1.5 mJ in Fig. 7(b). At low pump levels, the spatial distribution of N_2 takes the form of the pump power, whereas for high pump levels it tends to resemble the shape of the dopant concentration with z (i.e. more horizontal). As can be seen from these figures, the gain region is dependent on γ. It is limited to a short initial section of the fiber. Outside it, the light propagates with attenuation. As a consequence of this attenuation, ASE will be detected or not at the end of the fiber, depending on the total length and on the propagation losses. The gain lengths shown in Fig. 7(b) are shorter than most of the fiber lengths used in the experimental measurements, which explains the worsening of thresholds and efficiencies with L. On the other hand, by analyzing the spatial distribution of N_2 we can see whether the pumped energy can be above the ASE threshold or not. When it can be above it, there is an inflexion point in the curve at a certain distance z indicating that, at such position, amplification begins to occur, as can be seen in Fig. 7(b). The propagation losses in the rest of the fiber following this drop will determine if ASE is achieved or not at the end of the fiber. It must be noticed that the drop of N_2 occurs at deeper positions as the value of γ decreases. In contrast, if this inflexion point in the spatial distribution of N_2 indicating the onset of ASE does not occur, we are below the threshold regardless of the rest of the fiber, as happens in Fig. 7(a).

#193466 - $15.00 USD Received 5 Jul 2013; revised 6 Sep 2013; accepted 9 Sep 2013; published 3 Oct 2013

A simple and approximate calculation from Eqs. (2-3) for a single emission wavelength in stationary state gives the following expression for the pump-power threshold necessary to obtain a population-inversed state of the R6G molecules ($N_1 \approx N_2$):

$$P_p^{th'} = \frac{A_{core}(1-\beta)}{\sigma^a(\lambda_p)\tau\gamma}\left(h\frac{c}{\lambda_p}\right) \tag{5}$$

This expression indicates that an increase in the value of γ implies a diminishment in the threshold to achieve population inversion. This is in agreement with the behavior shown in Fig. 7(b), in which, for values of z at the beginning of the fiber, higher populations of N_2 are obtained as γ is increased. However, a high value of γ does not guarantee that population inversion will be achieved at the end of the fiber, because it does not take into account the fiber losses along L. Therefore, another ASE threshold for the fiber taking the losses into account should be derived. From Eqs. (1-3), in stationary state and neglecting the term containing β, we have worked out an approximate expression for this ASE threshold at a single emission wavelength λ_k, by considering $P \approx 0$ at threshold and equating the gain and the loss. The analytical result is the following one:

$$P_p^{th''}(L) = \frac{A_{core} N \sigma^a(\lambda_k)\left(h\frac{c}{\lambda_p}\right)L}{\tau\left(\sigma^a(\lambda_k)+\sigma^e(\lambda_k)\right)\left(1-\exp\left(\gamma N\sigma^a(\lambda_p)L\left(\frac{\sigma^a(\lambda_k)}{\sigma^a(\lambda_k)+\sigma^e(\lambda_k)}-1\right)\right)\right)} \tag{6}$$

In agreement with our results shown in Fig. 6(a), Eq. (6) explains the approximate linear variation of the threshold with L. In addition, it also yields lower thresholds for larger values of γ when L is sufficiently small. This is illustrated in Fig. 8, in which we have plotted the variation of $P_p^{th''}$ with L corresponding to a single emission wavelength (λ_k = 582 nm) for the three values of γ considered.

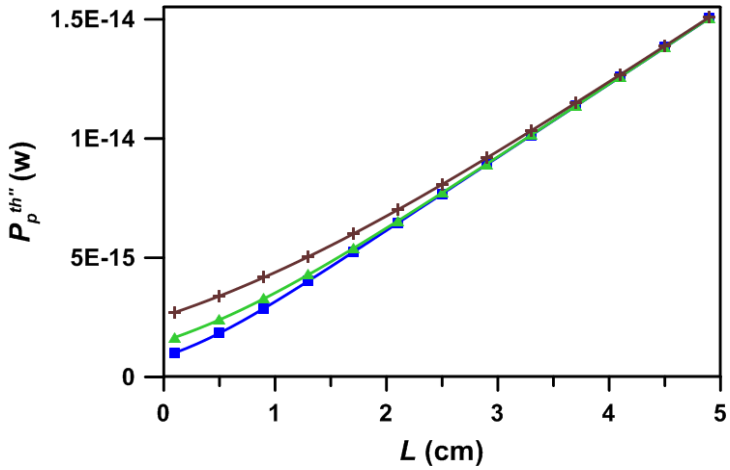

Fig. 8. Variation of threshold with fiber length obtained from Eq. (6). Solid line with crosses: curve with γ = 1. Solid line with triangles: curve with γ = 1.7. Solid line with squares: curve with γ = 3. The calculations have been performed with $A_{core} = \pi\ 0.3^2$ mm^2, τ = 4.8 ns, $N = 1.81 \times 10^{22}$ m^{-3}, $\sigma^a(\lambda_p = 532\text{nm}) = 4.27 \times 10^{-20}$ m^2, $\sigma^a(\lambda_k = 582\text{nm}) = 1.63 \times 10^{-20}$ m^2, and $\sigma^e(\lambda_k = 582\text{nm}) = 3.01 \times 10^{-21}$ m^2.

The dependence on L of the efficiency when the fiber is longer than the gain length is approximately given by the variation of the emission power with L. This can be explained from Eqs. (1-3) in stationary state by taking into account that, for such fiber lengths, N_2 / N_1 is

#193466 - $15.00 USD Received 5 Jul 2013; revised 6 Sep 2013; accepted 9 Sep 2013; published 3 Oct 2013

negligible and P_p becomes nearly constant. Therefore, for L significantly greater than the gain length, we can express the efficiency for an emission wavelength λ_k as follows:

$$\eta(L) = \frac{\Delta P}{\Delta P_p} = \frac{P(L)}{P_p(L)}\left(\frac{\sigma^a(\lambda_k) - \sigma^e(N_2/N_1)}{\sigma^a(\lambda_p)}\right) \propto P(L) \propto \exp(-\gamma\sigma^a(\lambda_k)N_1 L) \quad (7)$$

Taking into account this exponential behavior of the efficiency, we have fitted an exponential function to the experimentally obtained efficiencies in Fig. 6(b) in order to obtain the global fiber loss at all emitted wavelengths. The corresponding loss is $\alpha = 0.26$ cm^{-1}, with determination coefficient $R^2 = 0.98$. Similarly, we have obtained that the theoretical curves in Fig. 6(b) decay very approximately as exponential functions with the following losses: $\alpha = 0.12$ cm^{-1} for $\gamma = 1$, $\alpha = 0.21$ cm^{-1} for $\gamma = 1.7$ and $\alpha = 0.38$ cm^{-1} for $\gamma = 3$. Therefore, we can say that the best agreement between the experimental and the theoretical curves is obtained with $\gamma = 1.7$, as expected. Notice that the numerically calculated losses become greater as γ increases, in agreement with Eq. (7).

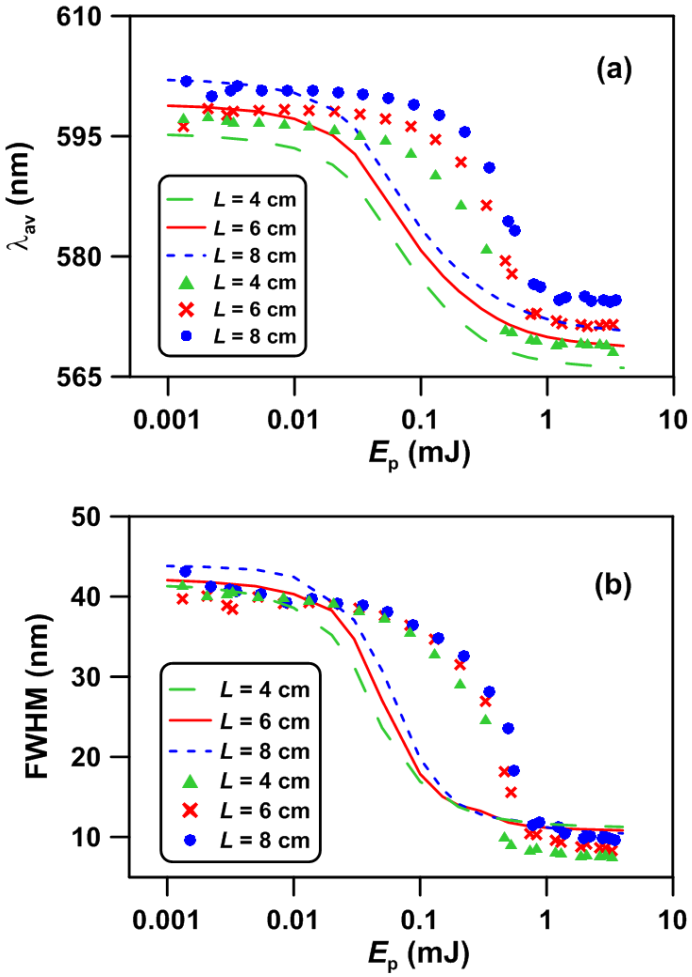

Fig. 9. (a) Shift of the average wavelength of the emission spectra and (b) narrowing of their widths as functions of the pump energy in our doped GI POFs for three fiber lengths. Symbols: experimental points. Solid and dashed lines: theoretical calculations with $\gamma = 1.7$. The same parameters as in Fig. 6 have been employed.

#193466 - $15.00 USD Received 5 Jul 2013; revised 6 Sep 2013; accepted 9 Sep 2013; published 3 Oct 2013

In Fig. 9 we show, for three different fiber lengths, the spectral behavior of the emission as a function of the pump energy, calculated numerically from Eqs. (1-3). We also include the corresponding experimental data. We can see that the theoretical curves predict well the amount of shift in the average wavelength and in the full width at half maximum of the output spectrum when the pump energies are increased around the ASE threshold. Besides, it can be observed that the abrupt drops of the theoretical curves are affected by L in a similar way as the experimental ones. Notice that the computationally obtained results present the abrupt shifts at lower pump powers than the experimental ones. This is in agreement with the lower threshold values predicted in Fig. 6(a). The theoretical average wavelengths plotted in Fig. 9(a) have been corrected to take into account that the absorption and emission cross sections in Eqs. (1-3) correspond to non-sufficiently short lengths of fiber. Ideally, they should correspond to a fiber length tending to cero. The estimated correction in a distance of about 2 cm is a blue shift of about 20 nm that compensates for the red shift that occurs in the short fiber distance employed for the cross sections. It must be mentioned that, just by changing the total fiber length employed for the fiber laser, it is possible to tune both the average wavelength of the output ASE and its FWHM.

Finally, Fig. 10 shows the photostability of the ASE intensity obtained from a doped fiber of L = 2.5 cm when it is pumped with 3 mJ for 2 hours. For this pump energy, which is well above the ASE threshold for the length L employed, the output energy still maintains about 40% of its initial value after two hours. In addition, we have observed that both the average wavelength of the ASE spectrum and its narrow FWHM remain unchanged during this pumping period. For the pumping conditions employed, we have not detected recovery in the emission intensity after letting the fiber rest for 3 days. However, for shorter pumping periods, of about 10 minutes, we have detected that the emission intensity is totally recovered in 3 days of rest.

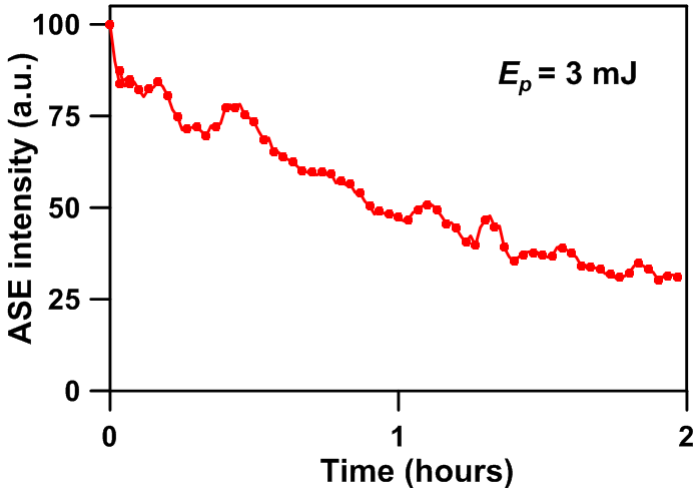

Fig. 10. Decrease of ASE intensity with time when the fiber is pumped with E_p = 3 mJ, for L = 2.5cm.

5. Summary

We have carried out a detailed study of the amplified spontaneous emission in a rhodamine-6G doped graded-index polymer optical fiber when it is pumped longitudinally. ASE effects such as blue shift of the emission average wavelength, spectral narrowing and rapid increase in the emission intensity have been observed experimentally for different fiber lengths. We have clearly shown that our theoretical model based on the laser rate equations can serve to describe the spectral ASE features successfully. On the other hand, the dependence on fiber length of ASE thresholds and efficiencies for all emission wavelengths has been also

#193466 - $15.00 USD Received 5 Jul 2013; revised 6 Sep 2013; accepted 9 Sep 2013; published 3 Oct 2013

analyzed, with satisfactory agreement between experimental and theoretical results. The effect of the overlapping factor between light power distribution and dopant concentration on ASE thresholds and efficiencies has been studied. A greater overlapping factor decreases the threshold for fiber lengths comparable to the gain lengths, shortens the optimum length for maximum efficiency and increases the slope of the exponential decay in the efficiency for long fibers.

Acknowledgments

This work has been sponsored by the institutions Ministerio de Economía y Competitividad under projects TEC2009-14718-C03-01, TEC2012-37983-C03-01, Gobierno Vasco/Eusko Jaurlaritza under projects AIRHEM-II, S-PE12CA001, IT664-13 and by the University of the Basque Country (UPV/EHU) through program UFI11/16. The work of I. Ayesta was supported in part by research fellowship from the University of the Basque Country (UPV/EHU), Vicerrectorado de Euskara y Plurilingüismo, while working on his Ph.D. degree. A part of this research is granted by the Japan Society for the Promotion of Science (JSPS) through the Funding Program for World-Leading Innovative R&D on Science and Technology (FIRST Program), initiated by the Council for Science and Technology Policy (CSTP).